Self-Assembly of Symmetric Diblock Copolymers Confined in Spherical Nanopores

Bin Yu,[†] Baohui Li,[*,†,‡] Qinghua Jin,[†] Datong Ding,[†] and An-Chang Shi[*,§]

College of Physics and Key Laboratory of Functional Polymer Materials, Ministry of Education, Nankai University, Tianjin, 300071, PR China, and Department of Physics and Astronomy, McMaster University, Hamilton, Ontario L8S 4M1, Canada

Received July 20, 2007; Revised Manuscript Received September 21, 2007

ABSTRACT: Self-assembly of symmetric diblock copolymers confined in spherical nanopores is studied using simulated annealing Monte Carlo simulations. The dependence of the self-assembled morphologies and chain conformations on the degree of confinement and the strength of the surface interactions is examined systematically. A rich variety of novel structures under the three-dimensional confinement has been revealed. As the strength of the surface preference is increased gradually from neutral to weakly preferential and finally strongly preferential to one of the blocks, the observed sequence of stable structures is from perpendicular lamellae to helices and/or embedded structures and finally to concentric-spherical lamellae. As the degree of confinement decreases, the stable region of the concentric-spherical lamellae becomes larger, while that of the embedded structures becomes smaller. For the structures obtained in spherical nanopores, corresponding counterparts in two-dimensional (2D) confined systems can be identified. On the other hand, the chain conformations of the three-dimensional (3D) confined structures are different from that of their corresponding 2D counterparts. A model is proposed which gives a reasonable description for the layer thicknesses of the concentric-lamellae in both 3D and 2D confined systems. Furthermore, in the limit of large pores, the model predictions for 3D and 2D confined systems are consistent with that observed in one-dimensional confined systems.

Introduction

Spontaneous formation of ordered nanostructures from self-assembly of block copolymers has attracted increasing recent interest. These ordered structures are of great scientific interests and they possess great potentials for technological applications.[1,2] Potential applications of block copolymer microstructures include lithographic templates for nanowires, photonic crystals, and high-density magnetic storage media. In most of the cases the block copolymer microphases are self-assembled in the bulk. On the other hand, it is of great interest to explore methods of producing microstructures that are not formed spontaneously in the bulk. One of these methods takes the advantage of confinement effects. It has been shown that nanoconfinement of block copolymers can be used to produce novel morphologies with potentially novel applications.[3] The influence of confinement on the microphase separation and morphology of block copolymers is also of fundamental interest in polymer science.[4]

The simplest confinement is one-dimensional (1D) in which the block copolymers are sandwiched between two flat, parallel surfaces. Symmetric (bulk lamella-forming) diblock copolymers under 1D confinement have been studied extensively. Experimental, theoretical and simulation studies have explored the effects of film thickness and surface preference to one or the other block on the resulting morphologies.[1,3,5,6] The interplay between confinement and surface preference causes deviations from the morphologies observed in the bulk. For the 1D confined block copolymers, much attention has been focused on controlling the orientation of the lamellae with respect to the confining surfaces. The basic results of these studies can be summarized as follows. When the surfaces are attractive to one of the blocks, in general lamellae parallel to the surfaces are preferred. However, when the spacing between the surfaces is incommensurate with the bulk lamellar spacing, it is possible to obtain lamellae perpendicular to the surfaces. The perpendicular lamellae are observed despite that one block prefers to the surfaces, as long as the surface preferential is weak enough. When the surfaces are neutral, perpendicular lamellae are preferred. Furthermore, it was found that for parallel lamellae, the lamellar period changes cyclically with film thickness around the bulk period L_0.[7,8]

A slightly more complicated form of confinement is realized when the copolymers are placed in cylindrical nanopores, leading to two-dimensional (2D) confined systems. Bulk lamella-forming diblock copolymers under 2D confinement have been extensively studied recently. When the pore diameter (D) is larger than the equilibrium period L_0 of the lamellae and the pore surface attracts one of the blocks, multiple set of concentric-cylindrical lamellae were observed in experiments,[9−13] as well as in theoretical studies[14] and simulations.[15−22] When D is comparable to L_0 and D/L_0 is not an integer, novel morphologies, such as stacked-disk or toroid, were observed experimentally.[10−11] For pores with neutral surfaces, lamellae normal to the pore axis (perpendicular lamellae or stacked-disk) were predicted in simulations.[16−22] For pores with weakly preferential surfaces for one of the blocks, novel morphologies, such as porous lamellar (mesh) morphologies, parallel lamellae as well as helices or mixed morphologies were predicted with simulations.[17−22]

Besides the equilibrium morphologies, the dependence of the chain conformations on the degree of confinement and the strength of the surface preference has been investigated for 2D confined diblock copolymer systems.[14,20,22] Furthermore, the dependence of the layer thicknesses on the degree of confinement has been examined for the rotationally symmetric concentric-

* Authors to whom correspondence should be addressed. E-mail: (B.L.) baohui@nankai.edu.cn; (A.-C.S.) shi@mcmaster.ca.
[†] College of Physics, Nankai University.
[‡] Key Laboratory of Functional Polymer Materials, Ministry of Education, Nankai University.
[§] Department of Physics and Astronomy, McMaster University.

10.1021/ma071624t CCC: $37.00
Published on Web 11/03/2007

cylindrical lamellae.[14,20,22] Using 2D self-consistent field theory (SCFT) calculations, Li et al. constructed phase diagrams of diblock copolymers under cylindrical confinement, and reported the variation of the layer thicknesses with the dimensionless pore diameter for the concentric lamellae.[14] They noticed that as the pore diameter increases, the lamellar spacing adjusts to fit the fixed number of lamellae into the pore and that, for larger pores, the structure in the inner region of the pore should be similar to that in the bulk.[14] Using both Monte Carlo simulations and the strong-stretching theory (SST), Wang studied the self-assembled morphology and the chain conformations of symmetric diblock copolymers confined in cylindrical nanopores systematically.[20] Wang also computed the layer thicknesses for the concentric-cylindrical lamellae, where good agreement was obtained between the two methods only on the thickness of the outermost A-rich layer. It is concluded that the SST has some deficiencies in describing the morphologies of 2D confined block copolymer systems.[20] Very recently, we studied the self-assembled morphology and the chain conformations of diblock copolymers confined in cylindrical nanopores.[22] On the basis of the assumption of constant interface area per chain, we proposed a simple model for the concentric-cylindrical lamellae, which gives a reasonable description of the layer thickness. However, it is found that there exist small deviations for the thickness from the simulated structures and the model predictions for the inner layers of the concentric-cylindrical lamellae when the number of A−B interfaces $n > 1$.[22]

For 2D confined self-assembly, studies have also been carried out for asymmetric diblock copolymers,[9,11,14,19,21,23−26] triblock copolymers,[27−28] diblock copolymer mixtures[29] and homopolymer/diblock copolymer mixtures.[30] Helical structures have been observed experimentally for the bulk cylinder-forming polystyrene-*b*-polybutadiene diblock copolymers.[11,23] Helices and stacked toroids have been predicted to spontaneously form inside cylindrical pores.[21,24−30] It is also found that the shape and size of the pores have a large effect on the structure and symmetry of the self-assembled morphologies.[9,26]

In contrast to the result of 1D confined self-assembly, more orientations (concentric-cylindrical lamellae, perpendicular lamellae and parallel lamellae) for lamellae and richer morphologies, which have no analogue in the bulk, have been obtained for diblock copolymers under 2D confinement. On the basis of this observation, it is expected that three-dimensional (3D) confined self-assembly of block copolymers may lead to novel morphologies different from those observed in 1D or 2D confined systems. However, to the best of our knowledge, few studies have been devoted in the self-assembly of block copolymers under 3D confinement.[15] In this paper, we present results of simulated annealing studies of the self-assembly of bulk lamella-forming diblock copolymers confined in spherical nanopores. We focused on the dependence of the self-assembled morphologies and the chain conformations on the degree of confinement and the strength of the surface preferences. We systematically vary the pore size and the interaction of the copolymer with the pore surface in smaller steps and wider ranges. A rich variety of novel structures in these 3D confined systems is predicted from our study. The predicted morphologies and the chain conformations will be compared with those obtained for the same copolymers confined in cylindrical pores. Furthermore, a new model describing the layer thickness for the concentric (spherical and cylindrical) lamellae is proposed. It is shown that this new model gives a more reasonable description of the layer thickness, as compared with our earlier simple model.[22] The basic assumptions behind the new model are examined.

Model and Methods

The computer simulations carried out in our study are based on a simulated annealing method and the "single-site bond fluctuation" model.[31,32] Our previous studies have established that the method and model are appropriate for studying the self-assembly of block copolymers in confined environment.[22,24,26,33] The model and algorithm are reviewed briefly below. A detailed description can be found elsewhere.[22,33]

Symmetric AB diblock copolymers of the form A_6B_6 are used in the study. The number of all the monomers in a copolymer chain is $N = 12$, while the number of the A and B monomers in a chain is $N_A = N_B = 6$, respectively, The volume fraction of the A-blocks is $f_A = {}^1/_2$. This particular model of diblock copolymers forms lamellae in the bulk. The period of the lamellae is found to be $L_0 = 9.33$ lattice spacing from our previous studies.[22] In the model, the bond length is set to 1 and $\sqrt{2}$ lattice spacing, thus each site has 18 nearest-neighbor sites. The total monomer concentration in the system is kept at a constant $\rho = 85\%$. Only repulsion between monomers occupied nearest neighbor sites separated with 1 and $\sqrt{2}$ lattice spacing is considered. In all cases, the repulsion between the A−B blocks is modeled by a nearest-neighbor interaction parameter $\epsilon_{AB} = 1.0k_BT_{ref}$, where k_B is the Boltzmann constant and T_{ref} is a reference temperature. Without loss of generality, the A−A and B−B interactions are set to zero, $\epsilon_{AA} = \epsilon_{BB} = 0$. Interactions between the vacancies and monomers are also set to zero. For simulations of confined self-assembly, the diblock copolymers are confined to a spherical pore of diameter D. The spherical pore is embedded in a cube of volume $V = L \times L \times L$ of a simple cubic lattice, where L is an integer which is larger than D. The surface preferences (characterized by the surface−polymer interactions, ϵ_{SA}andϵ_{SB}) have the form of $-\epsilon_{SA} = \epsilon_{SB} = \alpha\epsilon_{AB}$, where α is varied from 0 to 1 with small steps. The degree of confinement is represented by the parameter D/L_0, which is varied from small ($\sim$1.5) to quite large ($\sim$4.5) with small steps. The initial temperature and the annealing schedule are the same as that used previously.[22] Each Monte Carlo step (MCS) is defined as the time taken for, on average, all the lattice sites to be visited once. At each annealing step, we perform 25000 MCS per lattice site. At the final annealing step, we perform 15000 MCS per lattice site to equilibrate the system. After the equilibration period, we perform a further 10000 MCS per lattice site to sample. An ensemble of configurations is obtained by sampling one configuration every 10 MCS per lattice site. The various averages are evaluated using this ensemble of configurations.

Results and Discussion

In this section, we first present the self-assembled morphologies, and then the chain conformations as functions of the degree of confinement and the strength of the surface preferences. Typical morphologies as functions of D/L_0 and α are plotted in Figure 1, in which the A-blocks are shown in dark (red color) and the B blocks in light (green color). Similar to the case of cylindrical pores,[22] morphologies shown in Figure 1a are relatively simple for the two α limits, corresponding to very strong and very weak surface preferences. In the strong surface-preference limit, $\alpha \approx 1$, concentric-spherical lamellae (onionlike structures) are obtained. These structures occur in a relatively wider α range for larger pores (notice that the scale of α in Figure 1 is not uniform). Because of the strong surface-preference, the A-segments segregate to the surface, while the core of the concentric-spherical lamellae can be either A or B, depending on D/L_0. It is interesting to notice that the concentric-spherical lamellar structures exhibit a repeating pattern in the radial direction. At $D/L_0 \approx 2.0$, 3.1 and 4.2, one extra A−B interface is added to the structure. Thus, the repeat period for the concentric-spherical lamellae is about $1.1L_0$, slightly larger than L_0. Concentric-spherical lamellae were predicted several years ago by He et al. using Monte Carlo simulations in

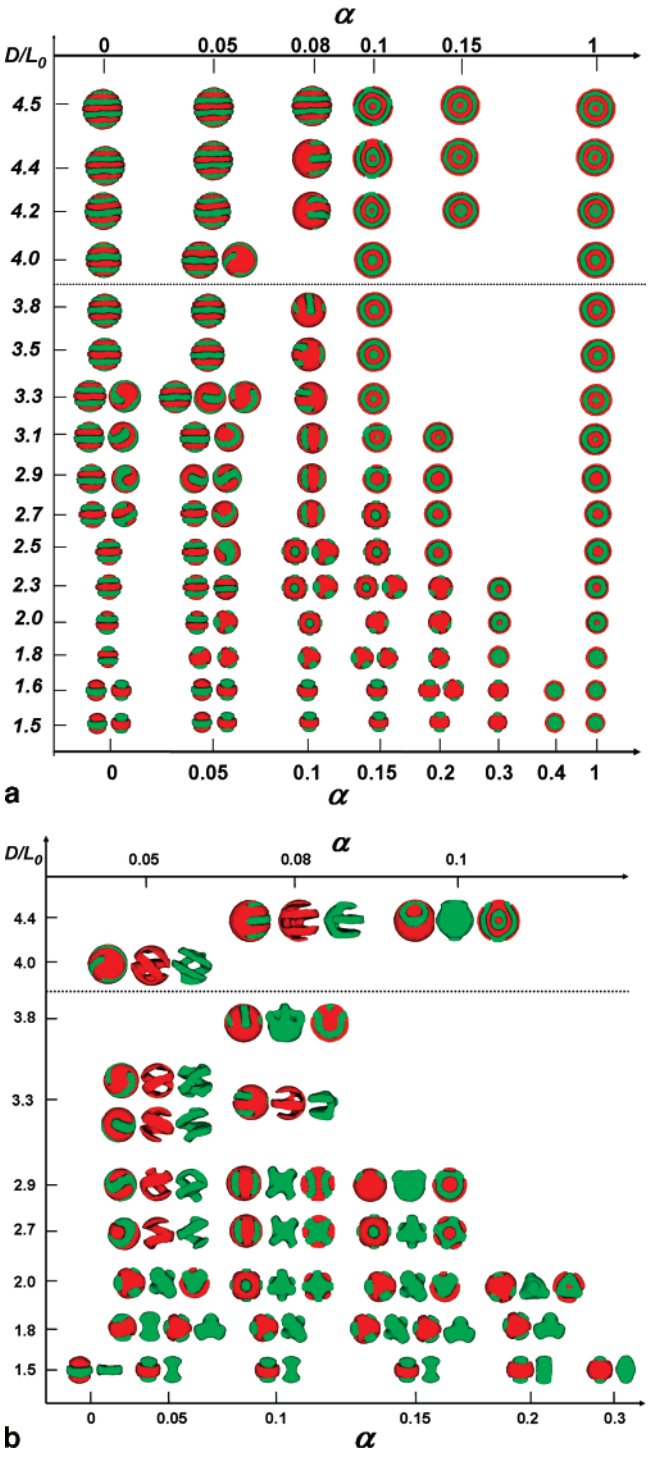

Figure 1. (a) Self-assembled morphologies for symmetric diblock copolymers confined in spherical pores as functions of the ratio D/L_0 and α, where for each concentric-spherical lamellar morphology, only a cross-section view is given and the boundary of the concentric-spherical lamellae is given with two identical structures at each D/L_0 value. (b) Some complex structures in Figure 1a, where the structure of A- domains, and the structure of B− domains or a cross-section view are also shown. In each Figure, the morphologies are corresponding to the lower α coordinate for $D/L_0 \leq 3.8$, and corresponding to the upper α coordinate for $D/L_0 > 3.8$.

spherical pores with strongly preferential surfaces,[15] consistent with our simulations.

In the limit of weak surface-preference, $\alpha \approx 0$, lamellae perpendicular to one of the pore axis (perpendicular lamellae) are observed as the dominating morphologies in the whole D/L_0 range. It is interesting to find that in each perpendicular lamellar structure with neutral surface, the average thickness for each A-rich or B-rich layer, defined as the ratio between the diameter of the pore and the number of layers in the structure, is in the range of $(0.50 \pm 0.05)\ L_0$ which is close to the thickness for each A-rich or B-rich layer in the bulk phase ($^1/_2L_0$). However, in the perpendicular lamellar structure, the thickness for each A-rich or B-rich layer is not identical. The thicknesses for the layers close to the pore surface are much thinner than those for the inner A-rich or B-rich layers, thus much smaller than $^1/_2L_0$. Therefore, the average thickness for the inner A-rich or B-rich layers is slightly thicker than $^1/_2L_0$, indicating that the copolymers can slightly change their conformation in order to adapt the environment. Detailed examinations of the morphology reveal that the A−B interfaces are not flat but undulate in the perpendicular lamellae even for neutral surfaces. This undulation may be the reason why the average thickness for the inner A-rich or B-rich layers is slightly larger than $^1/_2L_0$. Furthermore, for perpendicular lamellae with weakly preferential surfaces, the A−B interfaces are also undulated, where the thickness of the surface preferential A-rich layers is larger close to the pore surface and smaller at the pore center due to the surface preference. The thickness of the B-rich layers is larger at the pore center and smaller near to the pore surface.

As also shown in Figure 1, a rich variety of complex morphologies are obtained at intermediate α values. Some typical complex morphologies are plotted in Figure 1b, where the structure of B-domains and A-domains or a cross-section view are also shown for clarity. One feature at these intermediate α values is that embedded structures, where the A-segments form perforated concentric-spherical lamellae at the outermost layer, while the B-segments form structures with struts which are embedded in the holes of the A-domains, are frequently observed within smaller pores at $D/L_0 \leq 2.7$. For some very small pores with $D/L_0 \approx 1.5-1.6$, the embedded structures can even occur for neutral surfaces as degenerated structures with the perpendicular lamellae. For some pores with weakly preferential surfaces, embedded structures with different number of struts are obtained as mutually degenerated structures. For example, at $D/L_0 \approx 1.8$, embedded structures with two and three struts or with three and four struts are obtained as degenerated structures when $\alpha \approx 0.05$ and 0.15, respectively. Another example is found at $D/L_0 \approx 2.3-2.5$, where embedded structures with four and six struts are obtained as degenerated structures when $\alpha \approx 0.1$. The shape of each strut changes from a screw cap to a cylinder with a semisphere cap to a semi-elliptical sphere with the increase of α (Figure 1b). The number of struts (or holes) in the embedded structures can be 2, 3, 4, or 6, and it increases with the increase of D/L_0 at a given α value, such as with $\alpha \approx 0.1$, it is 2, 4, 6, and 6 or 4 at $D/L_0 \approx 1.5-1.6$, 1.8, 2.0, and 2.3−2.5, respectively. It also changes with α, such as at $D/L_0 \approx 1.8$, it is 2 or 3, 4, 4 or 3, and 3 with increasing α from 0.05 to 0.2. The distribution of the holes in the spherical surface of the pore can be highly symmetric. For structures with two holes at $D/L_0 \approx 1.5-1.6$, the two holes are distributed at the two poles of the sphere. For structures with three holes at $D/L_0 \approx 1.6-1.8$, the centers of the 3 holes may form a regular triangle. For structures with four or six holes at $D/L_0 \approx 1.8-2.5$, the centers of the holes may form a regular tetrahedron or a cube. For larger pores with $D/L_0 > 2.7$, similar structures sometimes can also occur but with defect, such as the embedded structure obtained at $D/L_0 \approx 4.5$ with $\alpha \approx 0.1$, which has five regular holes and the centers of the five holes should be five of the six apexes of a cubic; and at $D/L_0 \approx 4.4$ with $\alpha \approx 0.1$, or at $D/L_0 \approx 2.9-3.1$ with $\alpha \approx 0.15$, structures with only two

holes (not uniformly distributed) are obtained. And more frequently observed for larger pores, the holes are stripes in shape, such as these obtained at $D/L_0 \approx 2.7-3.1$ with $\alpha \approx 0.1$, where stripes of both A- and B-domains occur alternately at the pore surface. At $D/L_0 \approx 3.8$ with $\alpha \approx 0.1$, and $D/L_0 \approx 4.2-4.4$ with $\alpha \approx 0.08$, structures with a flower-basket shaped B-domains and a set of connected slabs for both A- and B-domains are obtained, respectively. With the increase of D/L_0, the region of the embedded structures becomes smaller.

The second feature at the intermediate α values is that helical structures are obtained for pores with weakly preferential surfaces with $D/L_0 \approx 2.5-3.3$ and 4.0, as well as for neutral pores with $D/L_0 \approx 2.7-3.3$. For the neutral pores, only single helices (S-helices) are observed, and they are degenerate structures with the perpendicular lamellae. On the other hand, for some pores with weakly preferential surfaces, S-helices and/or double helices (D-helices) are obtained, which are degenerate structures mutually and/or with the perpendicular lamellae. The two strands of the D-helices are usually connected together in one or two ends, such that the D-helical structure looks like a semi-eight or an eight. It is noticed that the pitch of the helices is much larger than L_0, and the radius of the helices is not a constant but changing with the position. The fact that the helical structures occur in a very narrow α range, indicates that they may be intermediate states between the perpendicular lamellae and the concentric−spherical lamellae. On the other hand, all the structures shown in Figure 1 are robust and reproducible. Simulations with several different random number generator seeds have been performed for each pore, and good reproducibility of the morphologies is obtained.

Similar to the case of cylindrical pores, we also computed the order parameter profiles to provide detailed information about the morphologies. Following Wang,[20] the order parameter profile is defined as $\psi(r) = \langle \varphi_A(r) - \varphi_B(r) \rangle / \langle \varphi(r) \rangle$, where $\varphi_i(r)$ (i = A or B) denotes the ratio of the number of the i-segments to the number of lattice sites in a collected configuration, $\varphi(r) = \varphi_A(r) + \varphi_B(r)$, $\langle\rangle$ denotes the ensemble average over all the collected configurations after equilibration, and rL_0 is a distance (r is the dimensionless distance). For concentric-spherical lamellae, the distance rL_0 changes from the pore surface to the pore center, whereas for perpendicular lamellae, it changes to the opposite surface along the symmetric axis of the structure. Thus, a fixed r describes a spherical shell for the concentric-lamellae, whereas it describes a circular disk for the perpendicular lamellae.

Parts a and b of Figure 2 show the order parameter profiles $\psi(r)$ with different D/L_0 values for the concentric-spherical lamellae at $\alpha = 1$ and the perpendicular lamellae at $\alpha = 0$, respectively. In Figure 2, the order parameter $\psi(r)$ oscillates between +1 and −1, indicating the alternating of A-rich and B-rich domains along the radial direction of the pore for the concentric-spherical lamellae, or along the symmetric axis direction for the perpendicular lamellae. Furthermore, we can clearly see in Figure 2 that the thickness of the A-rich and B-rich layers varies with both D/L_0 and the layer position in the structure. The thickness of the outermost A-rich layer is much smaller than those for the inner A-rich and B-rich layers. From the snapshot of the concentric-spherical lamellae of He et al., one can also observe that the thickness for the outermost surface preferential layer is much smaller than those for the inner A-rich or B-rich layers.[15] The shape of $\psi(r)$ in Figure 2a is square wave-like, indicating that the block copolymers at $\alpha = 1$ are in the strong segregation regime.[34] The shape of $\psi(r)$ in Figure 2b is neither sinusoidal nor quarewave-like, which is a result

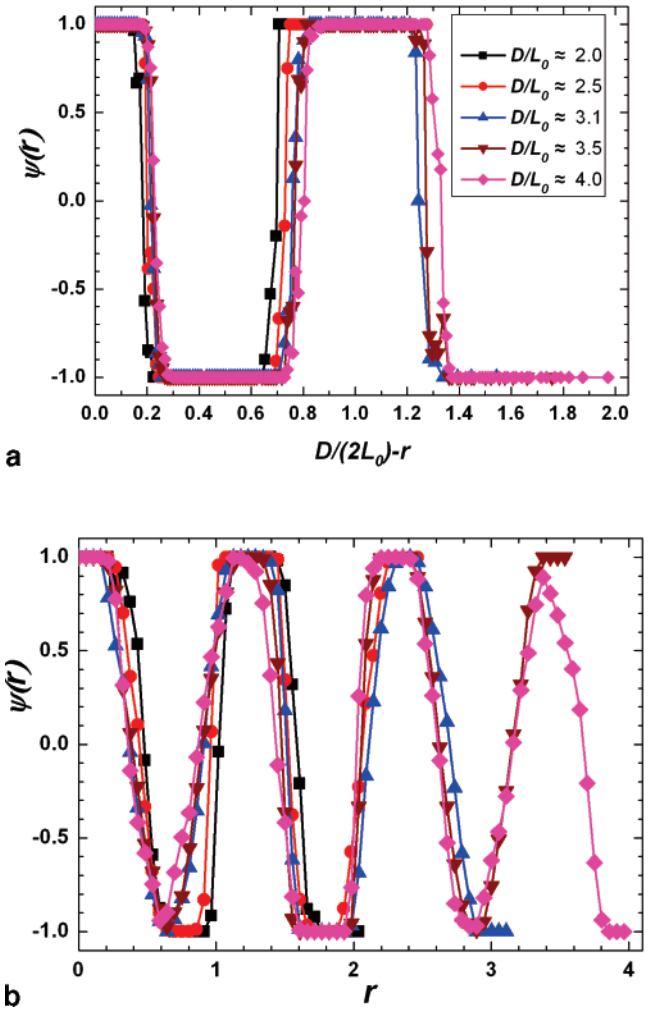

Figure 2. Order parameter profiles with different D/L_0 values for (a) the concentric-spherical lamellae at $\alpha = 1$ and (b) the perpendicular lamellae at $\alpha = 0$. The D/L_0 values are labeled in the legend of Figure 2a.

from the fact that the A−B interfaces are not flat but are undulated in the perpendicular lamellae.

The morphologies formed in the spherical nanopores can be compared with those obtained for symmetric diblock copolymers confined in cylindrical nanopores. Concentric-cylindrical lamellae in cylindrical pores were observed experimentally,[9−13] and predicted from theory[14] and simulations.[15−22] The concentric-spherical lamellae and concentric-cylindrical lamellae are from the same origin, i.e., the strong surface preference. It is interesting to notice that the transformation of the central domains from B (or A) to a central domain of A (or B) occurs at about the same D/L_0 values for these two types of concentric lamellae, when the same copolymers are confined in pores of spherical or cylindrical shapes with strongly preferential surfaces.[22] This coincidence indicates that these two structures have similar repeating periods in the radial direction. The perpendicular lamellae were also predicted from simulations in cylindrical pores with neutral or weakly preferential surfaces,[16−22] in which the thickness for each A-rich or B-rich layer in a perpendicular lamellar morphology is identical and equals to that for the bulk phase ($^1/_2L_0$) for the case of neutral surfaces. On the other hand, for the perpendicular lamellae in 3D confinement, the thickness is much smaller than $^1/_2L_0$ for the layers close to surfaces and is slightly larger than $^1/_2L_0$ for the inner layers. Another difference is that only perpendicular lamellae are obtained in cylindrical pores with neutral sur-

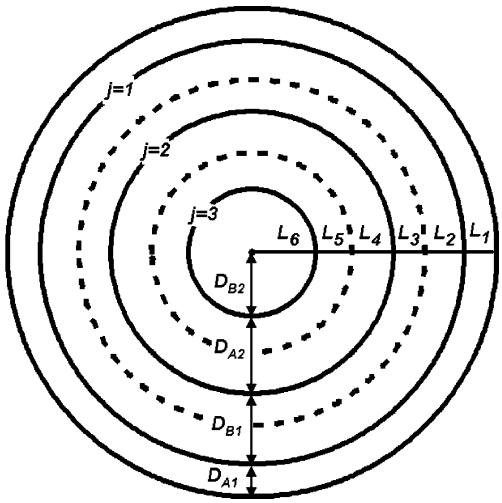

Figure 3. Schematics of concentric-spherical lamellae with $n = 3$. The outermost solid circle represents the pore surfaces, the inside solid circles represent A−B interfaces, and the dashed circles represent the assumed A−A or B−B interfaces in the strong segregation limit.

faces,[16,20,22] whereas embedded structures in smaller pores and S-helices in some pores are also predicted to occur for spherical pores with neutral surfaces. The helical structures, including both S-helices[17−19,21−22] and D-helices,[18,19,21] and mixed structures[20] were also predicted in cylindrical pores from simulations. However, the eight-shaped D-helices have never been observed in cylindrical pores. The embedded structures obtained in the spherical pores are similar to the catenarian structures obtained in the cylindrical pores.[22] However, the α or the D/L_0 range of the former is much larger than that of the latter.

In the case of cylindrical pores, we carried out a quantitative analysis for layer thickness of the concentric-cylindrical lamellae.[22] For the structures with the number of A−B interface $n = 1$, the thickness of the A-rich and B-rich layers can be predicted analytically based on the constraint that the volume of the A-rich layer is equal to that of the B-rich layer since the block copolymers are symmetric and incompressible. For the concentric-cylindrical lamellae with $n > 1$, an assumption of the constant interface area per chain is used to estimate the layer thicknesses analytically, besides the constraint on the volumes of the A-rich and the B-rich layers.[22] Good agreements are obtained for the layer thickness between the computed values from the simulated structures and the model predictions for both the A-rich and the B-rich layers when $n = 1$ and for the outermost A-rich layers when $n > 1$. However, small deviations between the model predictions and the computed values are found to exist for the thickness of the inner A-rich and B-rich layers when $n > 1$.[22]

The assumptions used in the case of concentric-cylindrical lamellae[22] can be tested in the case of concentric-spherical lamellae. Here, we will number the interfaces by $j = 1, 2, ..., n$, with $j = 1$ being closest to the pore surfaces. We number the outer and inner layers formed by the two blocks ending at the jth interface by L_i with $i = 2j - 1$ and $2j$, respectively (see Figure 3).[20,22] We use D_{mk} to denote the thickness of the kth m-rich layer, and the dimensionless layer thickness d_{mk}, is defined as $d_{mk} = D_{mk}/L_0$, where m = A or B and $k = 1$ being closest to the pore surfaces. On the basis of the constraint that the volume of the A-rich layer is equal to that of the B-rich layer, we can obtain the thickness of the A-rich and B-rich layers analytically for the concentric-spherical lamellae when $n = 1$

$$d_{A1} = \frac{D}{2L_0}\left(1 - \frac{1}{\sqrt[3]{2}}\right) \quad (1)$$

$$d_{B1} = \frac{1}{\sqrt[3]{2}}\frac{D}{2L_0} \quad (2)$$

For concentric-spherical lamellae with $n > 1$, the two constraints, constant volume and constant surface area, allow us to obtain the thickness of the A-rich and B-rich layers analytically. Specifically we have

$$\text{for } n = 2, \quad d_{A1} = \frac{D}{2L_0}\left(1 - \frac{\alpha}{\sqrt[3]{2(\alpha^3 - 1)}}\right),$$
$$d_{B1} = \frac{D}{2L_0}\frac{(\alpha - 1)}{\sqrt[3]{2(\alpha^3 - 1)}}, \quad \text{and } d_{A2} = \frac{D}{2L_0}\frac{1}{\sqrt[3]{2(\alpha^3 - 1)}}$$

$$\text{for } n = 3, \quad d_{A1} = \frac{D}{2L_0}\left(1 - \frac{\beta}{\sqrt[3]{2}\omega}\right), \quad d_{B1} = \frac{D}{2L_0}\frac{(\beta - \alpha)}{\sqrt[3]{2}\omega},$$
$$d_{A2} = \frac{D}{2L_0}\frac{(\alpha - 1)}{\sqrt[3]{2}\omega}, \quad \text{and } d_{B2} = \frac{D}{2L_0}\frac{1}{\sqrt[3]{2}\omega}$$

$$\text{for } n = 4, \quad d_{A1} = \frac{D}{2L_0}\left(1 - \frac{\gamma}{\sqrt[3]{2(\gamma^3 - \omega^3)}}\right),$$
$$d_{B1} = \frac{D}{2L_0}\frac{(\gamma - \beta)}{\sqrt[3]{2(\gamma^3 - \omega^3)}}, \quad d_{A2} = \frac{D}{2L_0}\frac{(\beta - \alpha)}{\sqrt[3]{2(\gamma^3 - \omega^3)}}$$
$$d_{B2} = \frac{D}{2L_0}\frac{(\alpha - 1)}{\sqrt[3]{2(\gamma^3 - \omega^3)}}, \quad \text{and } d_{A3} = \frac{D}{2L_0}\frac{1}{\sqrt[3]{2(\gamma^3 - \omega^3)}}$$

In the expressions, the constants are given by

$$\alpha = \frac{1}{3} + \frac{1}{3}(28 - 3\sqrt{87})^{1/3} + \frac{1}{3}(28 + 3\sqrt{87})^{1/3}$$

$$\beta = \frac{1}{3} + \left(\alpha^3 - \frac{26}{27} - \sqrt{(\alpha^3 - 1)\left(\alpha^3 - \frac{25}{27}\right)}\right)^{1/3} + \left(\alpha^3 - \frac{26}{27} + \sqrt{(\alpha^3 - 1)\left(\alpha^3 - \frac{25}{27}\right)}\right)^{1/3}$$

$$\omega^3 = \beta^3 - \alpha^3 + 1 \quad \text{and}$$
$$\gamma = \frac{1}{3} + \left(\omega^3 + \frac{1}{27} - \sqrt{\omega^3\left(\omega^3 + \frac{2}{27}\right)}\right)^{1/3} + \left(\omega^3 + \frac{1}{27} + \sqrt{\omega^3\left(\omega^3 + \frac{2}{27}\right)}\right)^{1/3}$$

From these expressions, we expect that all the layer thickness increases linearly with D. This is similar to the 2D case, although the slopes of the linear curves are much complex than that for the corresponding concentric-cylindrical lamellae.[22] Figure 4a compares the dimensionless thickness of the alternating A-rich and B-rich layers for the concentric-spherical lamellae computed from our simulation results with those predicted from the above equations. From Figure 4a, it is seen that there exist large differences for the thicknesses between the computed values from the simulated structures and the model predictions for the inner layers when $n > 1$. This result, along with that for the concentric-cylindrical lamellae,[22] indicates that the deviation of the model predictions from the simulated results increases with increasing A−B interfacial curvature, indicating a breakdown of the constant surface-area assumption. Therefore, it is desirable to seek other mechanisms to predict the layer thicknesses when $n > 1$.

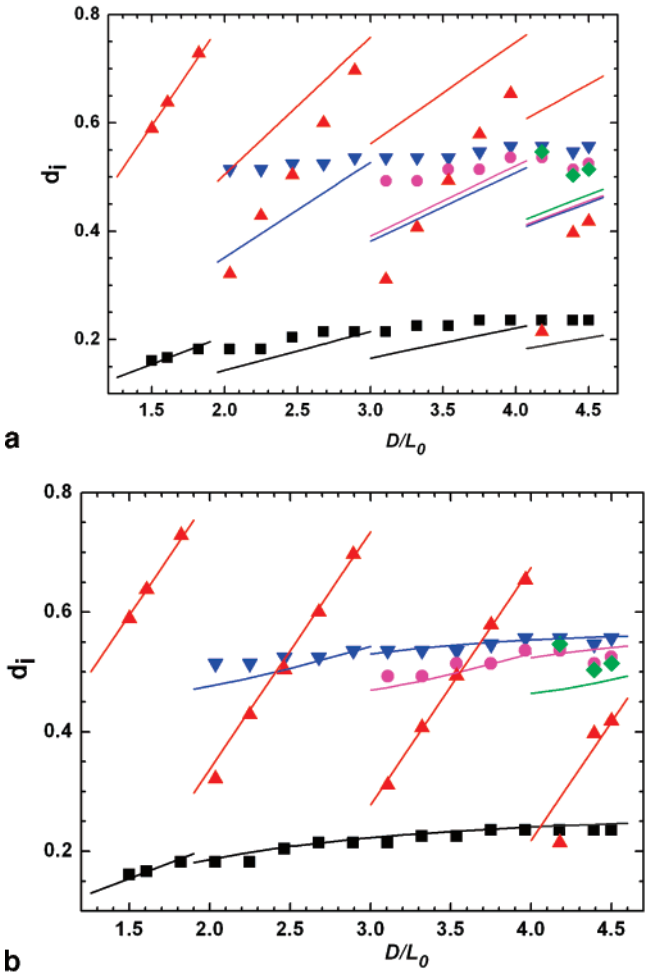

Figure 4. Comparison of the dimensionless thicknesses of the alternating A-rich and B-rich layers in concentric-spherical lamellae for strongly preferential surfaces at $\alpha = 1$ obtained from simulations (symbols) with those predicted from different models (curves or lines). In each figure, four parts according to D/L_0 from small to larger correspond to $n = 1$, 2, 3, and 4, respectively. In each part, the squares represent the thicknesses of the outermost A-rich layer d_{A1}. The up-triangles represent the thicknesses of the innermost A- or B− rich layers, and the down-triangles, circles and diamonds represent the thicknesses of d_{B1}, d_{A2}, and d_{B2}, respectively. (a) The model is based on the approach with the assumption of constant interface area per chain. In each part of the figure, the lines from low to up represent the thicknesses of d_{A1}, d_{B1}, d_{A2}, and d_{B2}, respectively. (b) The model is based on the approach proposed in the current work. In each part of the figure, the lowest curve (or line) represents the thickness of the outermost A-rich layer d_{A1}, the straight line with the largest slope represents the thickness of the innermost A- or B-rich layer and the other curves from up to low represent the thicknesses of d_{B1}, d_{A2}, and d_{B2}, respectively.

From the up-triangles (for the innermost layer thicknesses) in Figure 4a, we notice that when $n > 1$, the variation of the innermost layer thickness with D/L_0 is similar to that for $n = 1$. Motivated by this observation, we propose the following assumptions. For concentric-spherical lamellae when $n = 2$, we assume that as the innermost layer occurs in the structure, it increases with increasing D in the same way as that for $n = 1$. That is, when $n = 2$, the thickness for the innermost A-rich layer is just a displacement of eq 2. Thus, the thicknesses for the other A-rich and B-rich layers when $n = 2$ can be obtained on the basis of the constraint that the volume of the $(2j - 1)$th layer is equal to that of the $(2j)$th layer with knowing the thickness of the innermost A-rich layer. For concentric-spherical lamellae when $n = m$, we assume that the thickness for each of the inner $(m - 1)$ A-rich or B-rich layers increases with increasing D in the same way as that for the corresponding B-rich or A-rich layer when $n = m - 1$. Thus, we can obtain all the thicknesses of the A-rich and B-rich layers analytically when $n > 1$.

For $n = 2$,

$$d_{A1} = \frac{D}{2L_0}\left\{1 - \left[\frac{1}{2} + \frac{1}{2}\left(\frac{D - D_0}{D}\right)^3\right]^{1/3}\right\} \tag{3}$$

$$d_{B1} = \frac{1}{\sqrt[3]{2}}\frac{D}{2L_0}\left\{\left[1 + \left(\frac{D - D_0}{D}\right)^3\right]^{1/3} - \frac{D - D_0}{D}\right\} \tag{4}$$

$$d_{A2} = \frac{1}{\sqrt[3]{2}}\frac{(D - D_0)}{2L_0} \tag{5}$$

For $n = 3$,

$$d_{A1} = \frac{D}{2L_0}\left\{1 - \left[\frac{1}{2} + \frac{1}{2}\left(\frac{D - D_0}{D}\right)^3\right]^{1/3}\right\} \tag{6}$$

$$d_{B1} = \frac{1}{\sqrt[3]{2}}\frac{D}{2L_0}\left[1 + \left(\frac{D - D_0}{D}\right)^3\right]^{1/3} - \frac{1}{\sqrt[3]{2}}\frac{(D - D_0)}{2L_0}\left[1 + \left(\frac{D - 2D_0}{D - D_0}\right)^3\right]^{1/3} \tag{7}$$

$$d_{A2} = \frac{1}{\sqrt[3]{2}}\frac{(D - D_0)}{2L_0}\left\{\left[1 + \left(\frac{D - 2D_0}{D - D_0}\right)^3\right]^{1/3} - \left(\frac{D - 2D_0}{D - D_0}\right)\right\} \tag{8}$$

$$d_{B2} = \frac{1}{\sqrt[3]{2}}\frac{(D - 2D_0)}{2L_0} \tag{9}$$

For $n = 4$

$$d_{A1} = \frac{D}{2L_0}\left\{1 - \left[\frac{1}{2} + \frac{1}{2}\left(\frac{D - D_0}{D}\right)^3\right]^{1/3}\right\} \tag{10}$$

$$d_{B1} = \frac{1}{\sqrt[3]{2}}\frac{D}{2L_0}\left[1 + \left(\frac{D - D_0}{D}\right)^3\right]^{1/3} - \frac{1}{\sqrt[3]{2}}\frac{(D - D_0)}{2L_0}\left[1 + \left(\frac{D - 2D_0}{D - D_0}\right)^3\right]^{1/3} \tag{11}$$

$$d_{A2} = \frac{1}{\sqrt[3]{2}}\frac{(D - D_0)}{2L_0}\left[1 + \left(\frac{D - 2D_0}{D - D_0}\right)^3\right]^{1/3} - \frac{1}{\sqrt[3]{2}}\frac{(D - 2D_0)}{2L_0}\left[1 + \left(\frac{D - 3D_0}{D - 2D_0}\right)^3\right]^{1/3} \tag{12}$$

$$d_{B2} = \frac{1}{\sqrt[3]{2}}\frac{(D - 2D_0)}{2L_0}\left\{\left[1 + \left(\frac{D - 3D_0}{D - 2D_0}\right)^3\right]^{1/3} - \left(\frac{D - 3D_0}{D - 2D_0}\right)\right\} \tag{13}$$

$$d_{A3} = \frac{1}{\sqrt[3]{2}}\frac{(D - 3D_0)}{2L_0} \tag{14}$$

In these equations, D_0 is the repeat period of the concentric-spherical lamellae. As mentioned earlier, $D_0 \approx 1.1L_0$. When $n > 1$, only the thickness of the innermost A-rich or B-rich layers increases linearly with D. It is interesting to find that the thicknesses for the outermost A-rich layers with different n

coincide with a same curve when $n \geq 2$ (see eqs 3, 6, and 10), and that for the outermost B-rich layers they coincide with another curve when $n \geq 3$ (see eqs 7 and 11). It can also be shown that the thicknesses for the second A-rich layers with different n coincide with a third curve when $n \geq 4$, and so on.

Figure 4b compares the dimensionless thickness of the alternating A-rich and B-rich layers for the concentric-spherical lamellae computed from our simulation results with those predicted from the eqs 1−14 using $D_0/L_0 = 1.15$. Figure 4b shows that excellent agreement is obtained for layer thickness between the computed values and the model predictions. This agreement indicates that the proposed mechanism for layer thickness increasing with D/L_0 is a reasonable description for the simulated system. It also indicates that the exact repeating period for the concentric-spherical lamellae is $D_0 \approx 1.15$ in the simulated system. For all n, the variation of each innermost layer thickness with D/L_0 is linear for the computed values, which is consistent with the predictions. For the outermost A-rich layers, all the data points fall on the same curve, which is also consistent with the predictions.

The same assumptions proposed above for the concentric-spherical lamellae can be applied to the concentric-cylindrical lamellae when $n > 1$. The following equations for the layer thickness of the concentric-cylindrical lamellae are obtained.

For $n = 1$,

$$d_{A1} = \frac{D}{2L_0}\left(1 - \frac{1}{\sqrt{2}}\right) \quad \text{and} \quad d_{B1} = \frac{1}{\sqrt{2}}\frac{D}{2L_0}$$

For $n = 2$,

$$d_{A1} = \frac{D}{2L_0}\left\{1 - \left[\frac{1}{2} + \frac{1}{2}\left(\frac{D - D_0}{D}\right)^2\right]^{1/2}\right\},$$

$$d_{B1} = \frac{1}{\sqrt{2}}\frac{D}{2L_0}\left\{\left[1 + \left(\frac{D - D_0}{D}\right)^2\right]^{1/2} - \frac{D - D_0}{D}\right\}$$

and

$$d_{A2} = \frac{1}{\sqrt{2}}\frac{(D - D_0)}{2L_0}$$

For $n = 3$

$$d_{A1} = \frac{D}{2L_0}\left\{1 - \left[\frac{1}{2} + \frac{1}{2}\left(\frac{D - D_0}{D}\right)^2\right]^{1/2}\right\}$$

$$d_{B1} = \frac{1}{\sqrt{2}}\frac{D}{2L_0}\left[1 + \left(\frac{D - D_0}{D}\right)^2\right]^{1/2} - \frac{1}{\sqrt{2}}\frac{(D - D_0)}{2L_0}\left[1 + \left(\frac{D - 2D_0}{D - D_0}\right)^2\right]^{1/2}$$

$$d_{A2} = \frac{1}{\sqrt{2}}\frac{(D - D_0)}{2L_0}\left\{\left[1 + \left(\frac{D - 2D_0}{D - D_0}\right)^2\right]^{1/2} - \frac{D - 2D_0}{D - D_0}\right\},$$

$$\text{and } d_{B2} = \frac{1}{\sqrt{2}}\frac{(D - 2D_0)}{2L_0}$$

where D_0 is the repeating period of the concentric-cylindrical lamellae. Each of these equations is similar to the corresponding equation for the concentric-spherical lamellae. The only difference is that the cubic is replaced by the square and the cube root by the square root. Figure 5 compares the dimensionless thickness of the alternating A-rich and B-rich layers for the concentric-cylindrical lamellae computed from our simulation results with those predicted from the new model using $D_0/L_0 = 1.13$. Again excellent agreements are obtained for layer thickness between the computed values and the model predictions, indicating that the proposed mechanism for layer thickness increasing with D/L_0 is also reasonable for description concentric-cylindrical lamellae.

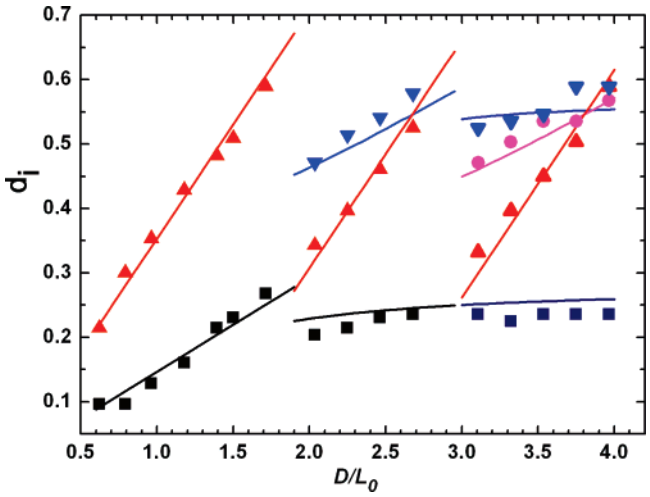

Figure 5. Comparison of the dimensionless thicknesses of the alternating A-rich and B-rich layers in concentric-cylindrical lamellae for strongly preferential surfaces at $\alpha = 1$ obtained from simulations[22] (symbols) with those predicted from the new model (lines or curves). In the figure, three parts according to D/L_0 from small to larger correspond to $n = 1$, 2, and 3, respectively. In each part, the squares and the lowest line or curve represent the thicknesses of the outermost A-rich layer d_{A1}. The up-triangles and the three straight lines with the largest slope represent the thicknesses of the innermost A- or B-rich layers. The others curves from up to low, and the down-triangles and circles represent the thicknesses of d_{B1} and d_{A2}, respectively.

The dimensionless layer thickness shown in Figure 4b can be compared with that of the concentric-cylindrical lamellae shown in Figure 5. It is noticed that there are similarities between the two cases. In both cases, the variation of the innermost layer thickness with D/L_0 is linear from the computed values, and the thicknesses of the outermost A-rich layers are always much smaller than those of the inner layers.[22] However, there are differences between the two cases. Since the thickness of both the A-rich and the B-rich layers is in good agreement with the model predictions based on the same constraints for the two cases, we can identify the differences between the two cases by comparing the corresponding equations. It is noticed that at a given D when $n = 1$, $d_{B1}$is larger while d_{A1} is smaller for the concentric-spherical lamellae than the corresponding quantity for the concentric-cylindrical lamellae since that the factor is $1/2^{1/3}$ in eqs 1 and 2 for the former while it is $1/\sqrt{2}$ for the latter.[22] Thus, the thickness of the innermost layer is always slightly larger for the concentric-spherical lamellae than that of the corresponding concentric-cylindrical lamellae. Compared with the assumption of constant interface area per chain used for the concentric-cylindrical lamellae,[22] it is likely that the mechanism for layer thicknesses increasing with D/L_0 proposed in this paper is more reasonable.

To examine the rational of the propose model of the layer thickness, we could examine whether these equations are physically sensible at limiting cases. As the thickness for the outermost A-rich layer, or for the outer B-rich or A-rich layers are given by the same curve for different n, when n is large, eqs 3, 7, and 12 are also valid. Therefore, we can use the first-order Taylor series expansion for the cubic or cube root terms in these equations when the pore is very large, i.e., D_0/D

approaches to zero. When D_0/D approaches to zero, $((D - D_0)/D)^3 = (1 - D_0/D)^3 \approx 1 - 3D_0/D$, thus $[1 + ((D - D_0)/D)^3]^{1/3} \approx (2 - 3D_0/D)^{1/3} \approx \sqrt[3]{2}\,(1 - D_0/2D)$. In a similar fashion, we have $[1 + ((D - 2D_0)/(D - D_0))^3]^{1/3} \approx \sqrt[3]{2}[1 - D_0/(2(D - D_0))]$ and $[1 + ((D - 3D_0)/(D - 2D_0))^3]^{1/3} \approx \sqrt[3]{2}[1 - D_0/(2(D - 2D_0))]$. Inserting these expansion formula into eqs 3, 7, and 12, we obtain

$$d_{A1} = \frac{D}{2L_0}\left\{1 - \left[\frac{1}{2} + \frac{1}{2}\left(\frac{D - D_0}{D}\right)^3\right]^{1/3}\right\} \approx \frac{D_0}{4L_0} \quad (15)$$

$$d_{B1} = \frac{1}{\sqrt[3]{2}}\frac{D}{2L_0}\left[1 + \left(\frac{D - D_0}{D}\right)^3\right]^{1/3} - \frac{1}{\sqrt[3]{2}}\frac{(D - D_0)}{2L_0}\left[1 + \left(\frac{D - 2D_0}{D - D_0}\right)^3\right]^{1/3} \approx \frac{D_0}{2L_0} \quad (16)$$

$$d_{A2} = \frac{1}{\sqrt[3]{2}}\frac{(D - D_0)}{2L_0}\left[1 + \left(\frac{D - 2D_0}{D - D_0}\right)^3\right]^{1/3} - \frac{1}{\sqrt[3]{2}}\frac{(D - 2D_0)}{2L_0}\left[1 + \left(\frac{D - 3D_0}{D - 2D_0}\right)^3\right]^{1/3} \approx \frac{D_0}{2L_0} \quad (17)$$

From eqs 15−17, we notice that $d_{A1} \rightarrow {}^1/_4$, $d_{B1} \rightarrow {}^1/_2$ and $d_{A2} \rightarrow {}^1/_2$, when D_0/D approaches zero and $D_0 \approx L_0$. That is, for very large pores, the thickness for the outermost layer of concentric-spherical lamellae approaches to $L_0/4$, and that for the middle layers approaches to $L_0/2$ if $D_0 \approx L_0$. These limiting results are identical to that for 1D confined systems, where symmetric diblock copolymers sandwiched between two flat strongly preferential surfaces and lamellae parallel to the surfaces are always obtained. In that case, the thickness for the outermost layer approaches to $L_0/4$, and that for the middle layers approaches to $L_0/2$ when the spacing between the surfaces is larger enough. Thus, in the limiting case when D_0/D approaches to zero, our predicted results for the outermost or the middle layer thicknesses in 3D confined system are consistent with those for 1D confined system. A similar analysis can be carried out for 2D confined system with the same conclusion. The small deviation of D_0 from L_0 in our results may be due to the relatively small pores used in our simulations, which is similar to the observation that in 1D confined systems, the lamellar period can slightly deviate from the bulk period L_0 when the spacing between the surfaces is small.[7,8] On the other hand, since the thickness for the middle A-rich or B-rich layer approaches $L_0/2$, the thickness of each L_i (see Figure 3) approaches $L_0/4$ for the middle layers. Thus, the thickness for the innermost layer L_{max} is larger than $L_0/4$ since that the volume of the L_{max} layer is equal to that of the $(L_{max} - 1)$ layer and the former is inside of the latter.

Figure 6 shows the mean-square end-to-end distance of the entire chain $\langle d_{EE}{}^2\rangle$ as a function of D/L_0 for the concentric lamellae with $\alpha = 1$ and the perpendicular lamellae with $\alpha = 0$. As a comparison, the bulk value is also plotted in the figure. The mean-square end-to-end distance is represented in units of the mean-square end-to-end distance of the corresponding ideal Gaussian chain ($=Nb^2$, where $b^2 \approx 1.6285$ is the square of the average of all the allowed bond length and N is the corresponding chain length). In Figure 6, the difference in $\langle d_{EE}{}^2\rangle$ between the two cases with different α values is large. For the case of strongly preferential surfaces ($\alpha = 1$), all the $\langle d_{EE}{}^2\rangle$ values are smaller than the bulk value, indicating that the chains are always compressed relative to the unconfined chains. The reason for this is the same as that mentioned in the case of cylindrical pores,[22] where chains close to the surface are compressed since

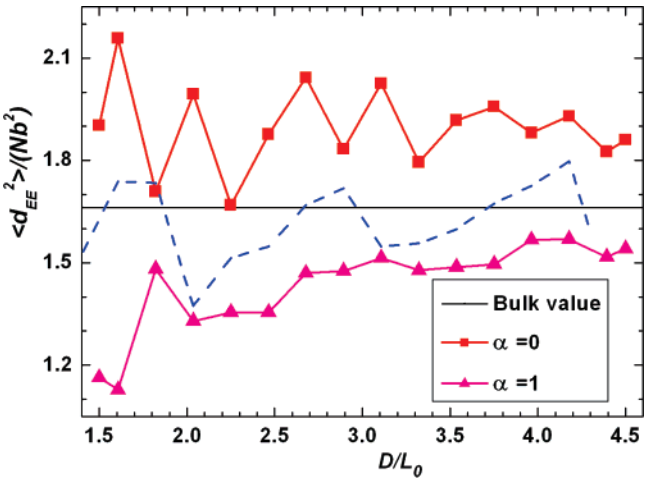

Figure 6. Mean- square end-to-end distance, $\langle d_{EE}{}^2\rangle$, as a function of D/L_0 for the concentric lamellae with $\alpha = 1$ and the perpendicular lamellae with $\alpha = 0$. The symbols and the solid curves correspond to the case of spherical pores, and the dashed curve corresponds to the case of the concentric- cylindrical lamellae.

they cannot interpenetrate with other chains from the outward radial direction due to the existence of the surfaces. The increase of $\langle d_{EE}{}^2\rangle$ with increasing D/L_0 is due to the fact that the fraction of the chains close to the surfaces is becoming smaller with the increase of D/L_0. It is also notice that there are jumps in $\langle d_{EE}{}^2\rangle$ at $D/L_0 \approx 2.0$, 3.3, and 4.3 which are close to the values where the system transforms the central domains. The jumping points separate the $\langle d_{EE}{}^2\rangle$ curve into four parts which corresponds to $n = 1$, 2, 3, and 4, respectively. In each part, $\langle d_{EE}{}^2\rangle$ increases with D/L_0, and the slope of $\langle d_{EE}{}^2\rangle$ for each part decreases with the increase in n, which resembles to the variations of the layer thicknesses for the outer layers shown in Figure 4.

For the perpendicular lamellae with $\alpha = 0$, $\langle d_{EE}{}^2\rangle$ is always larger than the bulk value, and oscillates with increasing D/L_0. The larger $\langle d_{EE}{}^2\rangle$ value for the perpendicular lamellae indicates that the chains are always stretched relative to the unconfined chains. It stems from the fact that the thickness is larger than ${}^1/_2L_0$ for the inner A-rich or B-rich layers and that the A−B interfaces are undulated. The oscillation of $\langle d_{EE}{}^2\rangle$ with increasing D/L_0 corresponds to the variation of the number of A−B interfaces in the perpendicular lamellae. At a given number of A−B interfaces, $\langle d_{EE}{}^2\rangle$ increases almost linearly with increasing D/L_0.

Figure 7 shows the mean-square end-to-end distance of the two individual blocks $\langle d_{EEA}{}^2\rangle$ and $\langle d_{EEB}{}^2\rangle$, as a function of D/L_0 for the concentric lamellae with $\alpha = 1$, where the bulk value is also plotted. Each of the quantities is also represented in units of the mean-square end-to-end distance of the ideal Gaussian chain. It is noticed that $\langle d_{EEA}{}^2\rangle$ is always much smaller than the corresponding $\langle d_{EEB}{}^2\rangle$ and also always smaller than the bulk value. The difference between $\langle d_{EEB}{}^2\rangle$ and $\langle d_{EEA}{}^2\rangle$ originates from the fact that the A-blocks occupy the outermost region in the pore. As shown in Figure 4, the thickness of the outermost A-rich layer is always smaller than that for the inner A-rich or B-rich layers, and also smaller than the corresponding bulk value (${}^1/_4$). For smaller pores, it is much smaller than 1/4. Thus, the A-chains in the outermost layer are much compressed relative to the inner chains or chains in the bulk. This can explain why $\langle d_{EEA}{}^2\rangle$ values are always much smaller than the corresponding $\langle d_{EEB}{}^2\rangle$ values and also always smaller than the bulk value. On the other hand, as also shown in Figure 4, the thickness of all the B-rich layers is always larger than the corresponding bulk value (for the innermost B-rich layers, the corresponding bulk

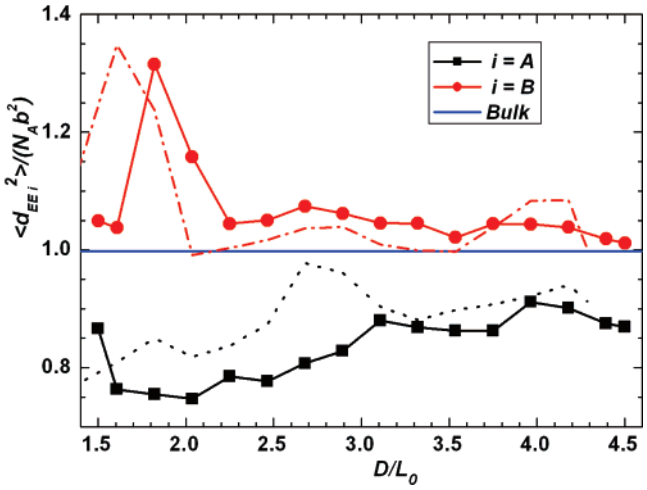

Figure 7. Mean-square end-to-end distances for A and B chains, $\langle d_{EEA}^2 \rangle$ and $\langle d_{EEB}^2 \rangle$, respectively, as a function of D/L_0 for strongly preferential surfaces. The symbols and the solid curves correspond to the case of spherical pores, and the dashed and dotted curves are for the case of cylindrical pores.

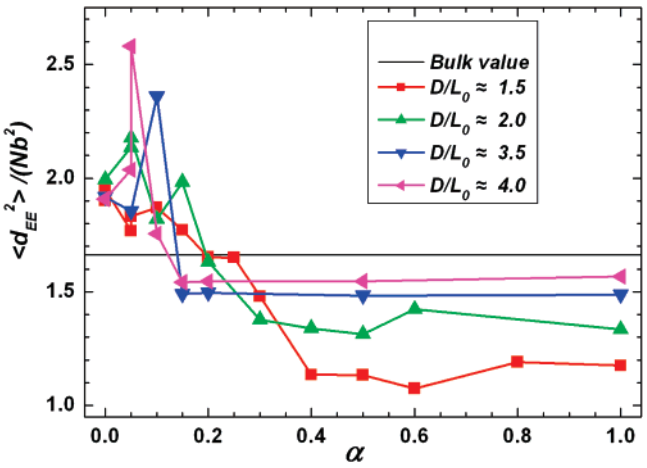

Figure 8. Mean-square end-to-end distances as a function of α, where the values for the degenerated structures are all shown.

value is $^1/_4$ because the innermost layer is an isolated layer, whereas for the other B-rich layers, the corresponding bulk value is $^1/_2$), and sometimes much larger than the corresponding bulk value. Thus, the B-chains are always stretched relative to the chains in the bulk, which can explain why $\langle d_{EEB}^2 \rangle$ is always larger than the corresponding bulk value.

Figure 8 shows the variation of $\langle d_{EE}^2 \rangle$ with α, and the corresponding bulk value is also shown. We see that all the $\langle d_{EE}^2 \rangle$ curves have a similar trend: at $\alpha = 0$, the value of $\langle d_{EE}^2 \rangle$ is slightly larger than the bulk value; there is a peak at a smaller α value; after that the value of $\langle d_{EE}^2 \rangle$ is very close to that at $\alpha = 1$. The values of $\langle d_{EE}^2 \rangle$ at $\alpha = 0$ and $\alpha = 1$ depend on D/L_0 (see Figure 6). The peak of the $\langle d_{EE}^2 \rangle$ curve corresponds to the helical structures with larger periods or embedded structures, and is shifted to a smaller α value with the increase of D/L_0.

The computed mean-square end-to-end distances for the 3D confined system can be compared with those obtained for the same copolymers under 2D confinement. The $\langle d_{EE}^2 \rangle$, $\langle d_{EEA}^2 \rangle$, and $\langle d_{EEB}^2 \rangle$ for the concentric-cylindrical lamellae in the 2D confined system with strongly preferential surfaces[22] are also plotted in Figure 6 and 7 with dashed or dotted lines, respectively. From Figure 6, we see that with strongly preferential surfaces, chains are more compressed in the 3D confined system than those in the 2D confined system, which is because

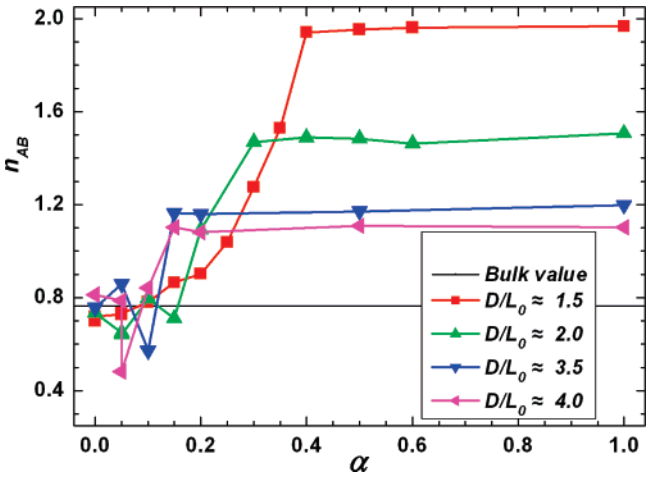

Figure 9. Average contact numbers for an A-monomer with B-monomers as a function of α, where the values for the degenerated structures are all shown.

that at a given pore diameter D, the fraction of chains close to the surface is larger for the concentric-spherical lamellae than that for the concentric-cylindrical lamellae, and that the chains close to the surface are more compressed. This can be estimated for a given pore diameter D. The fraction of chains close to the surface is proportional to the ratio between the surface area and the volume, thus, it is proportional to 6/D for a spherical pore while it is 4/D for a cylindrical pore. The larger fraction of chains close to the surface is the reason that chains are more compressed in the concentric-spherical lamellae. From Figure 7, we see that it is the surface preferential A-chains that are more compressed in the concentric-spherical lamellae. We also see that the B-chains are more stretched slightly than that in the concentric-cylindrical lamellae, which is consistent with that predicted from the layer thicknesses, where it is predicted that at a give D when $n = 1$, d_{B1} is larger for the concentric-spherical lamellae than that for the concentric-cylindrical lamellae. On the other hand, we notice that chains are more stretched in the perpendicular lamellar morphology with neutral surfaces for the 3D confined system than those for the 2D confined system, since that the former is always larger than the bulk value whereas the latter is always smaller than the bulk value.[22] In the perpendicular lamellar morphology, chains are more stretched for the 3D confined system though the fraction of chains close to the surface is larger, which is because of the thicker layer thicknesses for the inner layers in the perpendicular lamellar morphology in the 3D confined system mentioned above.

Figure 9 shows the variation of n_{AB}, the average contact number for an A-monomer with B-monomers, with α, and also with the bulk value. We see that all the n_{AB} curves also have a similar trend: the value of n_{AB} is very close to the bulk value for neutral surfaces, there is a downward peak at a smaller α value, and after that the value of n_{AB} is very close to that at $\alpha = 1$ which is much larger than the bulk value. Comparing with Figure 8, we notice that each curve of n_{AB} at a given D/L_0 value is just a reverse version of the corresponding curve of $\langle d_{EE}^2 \rangle$. Therefore, it is the interface energy for contact between A−B domains that are favorable for the formation of complex morphologies at smaller α values and compensated the entropic loss in these morphologies. Comparing with the results obtained for the same copolymers under 2D confinement,[22] we notice that at a given D, n_{AB} is higher for the concentric-spherical lamellae than that for the concentric-cylindrical lamellae. The reason for this is originated from the larger ratio between the

interface area and the volume for the concentric-spherical lamellae.

Conclusions

We have performed lattice simulated annealing simulations to study the self-assembly of bulk lamella-forming AB diblock copolymers confined in spherical nanopores. We have systematically investigated the dependence of the self-assembled morphologies and the chain conformations on the degree of confinement and the strength of the surface preference, which are characterized by the parameter D/L_0 and α, respectively. We have identified a sequence of novel structures under this 3D confinement. In addition to visual inspection of the morphologies, the ensemble-averaged order parameter profiles, the mean-square end-to-end distances for the whole chain and for the A and the B chains, and the average contact number for an A-monomer with B-monomers are used to provide detailed information about the system. The observed self-assembled structures and the chain conformations are compared with those obtained for the same copolymers confined in cylindrical nanopores.

For strongly preferential surfaces at large α, concentric-spherical lamellae with rotational symmetry are obtained, in which the number of A−B interfaces depending on D/L_0. It is shown that the model, based on the assumption of the constant interface area per chain used previously for describing the layer thickness of the concentric-cylindrical lamellae, cannot describe the layer thickness of the concentric-spherical lamellae well. The layer thickness for the simulated concentric-spherical (or cylindrical) lamellae can be well described by a new model which is based on the assumption that in larger pores, the layer thickness for each of the inner layers increases with D/L_0 *in the same way as that* for the corresponding layer in the smaller pores. Excellent agreements for the layer thicknesses between the computed values and the model predictions are obtained, which indicates that the proposed mechanism for the layer thicknesses with increasing D/L_0 is a reasonable description for the simulated system. Furthermore, in the limit of large pore, the predict results from the new model for 3D or 2D confined systems are consistent with those for 1D confined system. The mean-square end-to-end distance of the entire chain is smaller for the concentric-spherical lamellae than that for the concentric-cylindrical lamellae, and also smaller than the bulk value, whereas the average contact number is much larger for the former than that for the latter, and also much larger than the bulk value.

For neutral surfaces with $\alpha = 0$, perpendicular lamellae can be obtained regardless of D/L_0. The thicknesses for the layers close to the pore surface in each perpendicular lamellar morphology are much smaller than those for the inner layers, while the average thicknesses for the inner A-rich or B-rich layers are slightly larger than $^1/_2L_0$ (the bulk value). In this case, the mean-square end-to-end distance of the entire chain is always larger than the bulk value, and also larger than that for the corresponding morphology in the cylindrical pores.

For weakly preferential surface, a rich variety of complex morphologies are predicted. For most of these morphologies such as helical structures, their periods are much larger than L_0, which results in that the chains are more stretched for weakly preferential surfaces than the bulk chains or the chains within pores of strongly preferential surfaces. It is also found that the interface energy compensated the entropic loss in the complex morphologies. The embedded structures and S-helices are also obtained for some neutral surfaces as degenerated structures for the perpendicular lamellae.

Acknowledgment. This research was supported by the National Natural Science Foundation of China (Grant Nos. 20474034, 20774052, 20374031, and 20373029), by the Chinese Ministry of Education with the Program of New Century Excellent Talents in University and the Program of the Joint-Research Foundation of the Nankai and Tianjin Universities (Grants No. NCET-05-0221), and by Nankai University ISC. A.-C.S. acknowledges the supports by the Natural Science and Engineering Council (NSERC) of Canada.

References and Notes

(1) Park, C.; Yoon, J.; Thomas, E. L. *Polymer* **2003**, *44*, 6725.
(2) Hamley, I. W. *Nanotechnology* **2003**, *14*, R39.
(3) Wang, Q. In *Nanostructured Soft Matter: Experiment, Theory, Simulation and Perspectives*; Zvelindovsky, A. V., Ed.; Springer: Berlin, 2007; Chapter 16.
(4) Gelb, L. D.; Gubbins, K. E.; Radhakrishnan, R.; Sliwinska-Bartkowiak, M. *Rep. Prog. Phys.* **1999**, *62*, 1573.
(5) Binder, K.; Muller, M. *Curr. Opin. Colloid Interface Sci.* **2000**, *5*, 314.
(6) Fasolka, M. J.; Mayes, A. M. *Annu. Rev. Mater. Sci.* **2001**, *31*, 323.
(7) Lambooy, P.; Russell, T. P.; Kellogg, G. J.; Mayes, A. M.; Gallagher, P. D.; Satija, S. K. *Phys. Rev. Lett.* **1994**, *72*, 2899.
(8) Koneripalli, N.; Singh, N.; Levicky, R.; Bates, F. S.; Gallagher, P. D.; Satija, S. K. *Macromolecules* **1995**, *28*, 2897.
(9) Xiang, H.; Shin, K.; Kim, T.; Moon, S. I.; McCarthy, T. J.; Russell, T. P. *Macromolecules* **2004**, *37*, 5660.
(10) Shin, K.; Xiang, H.; Moon, S. I.; Kim, T.; McCarthy, T. J.; Russell, T. P. *Science* **2004**, *306*, 76.
(11) Xiang, H.; Shin, K.; Kim, T.; Moon, S. I.; McCarthy, T. J.; Russell, T. P. *J. Polym. Sci., Part B: Polym. Phys.* **2005**, *43*, 3377.
(12) Sun, Y.; Steinhart, M.; Zschech, D.; Adhikari, R.; Michler, G. H.; Goele, U. *Macromol. Rapid Commun.* **2005**, *26*, 369.
(13) Ma, M.; Krikorian, V.; Yu, J. H.; Thomas, E. L.; Rutledge, G. C. *Nano. Lett.* **2006**, *6*, 2969.
(14) Li, W.; Wickham, R. A.; Garbary, R. A. *Macromolecules* **2006**, *39*, 806.
(15) He, X.; Song, M.; Liang, H.; Pan, C. *J. Chem. Phys.* **2001**, *114*, 10 510.
(16) Sevink, G. J. A.; Zvelindovsky, A. V.; Fraaije, J. G. E. M.; Huinink, H. P. *J. Chem. Phys.* **2001**, *115*, 8226.
(17) Chen, P.; He, X.; Liang, H. *J. Chem. Phys.* **2006**, *124*, 104906.
(18) Feng, J.; Ruckenstein, E. *Macromolecules* **2006**, *39*, 4899.
(19) Feng, J.; Ruckenstein, E. *J. Chem. Phys.* **2006**, *125*, 164911.
(20) Wang, Q. *J. Chem. Phys.* **2007**, *126*, 024903.
(21) Feng, J.; Liu, H. L.; Hu, Y. *Macrom. Theory Simul.* **2006**, *15*, 674.
(22) Yu, B.; Sun, P.; Chen, T.; Jin, Q.; Ding, D.; Li, B.; Shi, A.-C. *J. Chem. Phys.* **2007**, *127*, 114906.
(23) Xiang, H.; Shin, K.; Kim, T.; Moon, S. I.; McCarthy, T. J.; Russell, T. P. *Macromolecules* **2005**, *38*, 1055.
(24) Yu, B.; Sun, P.; Chen, T.; Jin, Q.; Ding, D.; Li, B.; Shi, A.-C. *Phys. Rev. Lett.* **2006**, *96*, 138306.
(25) Li, W.; Wickham, R. A. *Macromolecules* **2006**, *39*, 8492.
(26) Yu, B.; Sun, P.; Chen, T.; Jin, Q.; Ding, D.; Li, B.; Shi, A.-C. *J. Chem. Phys.* **2007**, *126*, 204903.
(27) Xiao, X.; Huang, Y. M.; Liu, H. L.; Hu, Y. *Macrom. Theory Simul.* **2007**, *16*, 166.
(28) Feng, J.; Ruckenstein, E. *J. Chem. Phys.* **2007**, *126*, 124902.
(29) Zhu, Y.; Jiang, W. *Macromolecules* **2007**, *40*, 2872.
(30) Wu, Y.; Cheng, G.; Katsov, K.; Sides, S. W.; Wang, J.; Tang, J.; Fredrickson, G. H.; Moskovits, M.; Stucky, G. D. *Nat. Mater.* **2004**, *3*, 816.
(31) Carmesin, I.; Kremer, K. *Macromolecules* **1988**, *21*, 2819.
(32) Larson, R. G. *J. Chem. Phys.* **1992**, *96*, 7904. Larson, R. G. *J. Chem. Phys.* **1989**, *91*, 2479.
(33) Yin, Y.; Sun, P.; Chen, T.; Li, B.; Jin, Q.; Ding, D.; Shi, A.-C. *Chem. Phys. Chem* **2004**, *5*, 540.
(34) Wang, Q.; Nealey, P. F.; de Pablo, J. J. *Macromolecules* **2002**, *35*, 9563.

MA071624T